THE USE OF STODOLA MODES IN ROTOR-BLADE AEROELASTIC STUDIES

by

A. Simpson
Flight Dynamics Division
RAE Bedford, UK

Abstract

Stodola modes for a non-rotating, non-uniform blade are derived from the uncoupled lead-lag, flap and torsion eigenfunctions of a corresponding uniform blade by use of a single step of Stodola's method. When used as assumed modes for the non-rotating blade, they have been shown to exhibit remarkable convergence properties. In this paper, Stodola modes, orthogonalised by the Rayleigh-Ritz method, are used in the various stages of an aeroelastic formulation for a rotor (in hover) comprising semi-rigid blades. It is shown that the basic non-rotational Stodola modes may be used to formulate the Lagrangian equations of motion of a 'rotational basis system', the eigenvalues of which, once more, exhibit excellent convergence properties. The fully coupled eigenfunctions of the rotational basis system are then used as normal modes in the aeroelastic formulation. Hover trim states and aeroelastic eigenvalues are studied with respect to the number of retained normal modes.

The work described herein comprises the first stage of the implementation of a modal Lagrangian rotor theory which is to be used in flying qualities and active control investigations for rotorcraft of all types.

Notation

$\mathbf{A}$	classical inertia matrix.
$\mathbf{B}$	(or $\Omega\mathbf{B}$) gyroscopic matrix.
$\mathbf{C}$	(or $\Omega^2\mathbf{C}$) centrifugal stiffness matrix.
$\mathbf{D}$	lag/structural damping matrix.
$\mathbf{E}$	elastic matrix.
$EI(s)$	local flexural rigidity.
$\mathbf{f}$	$= \{f_1(s)\ ,\ f_2(s)\ ,\ \ldots\}$, column vector of lead-lag modes.
$\mathbf{F}$	$= \{F_1(s)\ ,\ F_2(s)\ ,\ \ldots\}$, column vector of flap modes.
$GJ(s)$	local torsional rigidity.
$\mathbf{h}$	$= \{h_1(s)\ ,\ h_2(s)\ ,\ \ldots\}$, column vector of torsion modes.
$h_0(s)$	rigid-body pitch mode.
k	pcu effective stiffness.
$k_p(s)$	pitch radius of gyration about blade flexural axis at s .
ℓ	blade span.
m	number of rotational Stodola/R-R modes retained in the aero-elastic analysis.
$m(s)$	local mass/unit length.
n	matrix order: basic Stodola mode formulation.
$\bar{n}$	$= p_\ell + p_f + p_t + 1$: matrix order - rotational basis system.
n_B	number of blades.
N	number of spanwise integration intervals.
p	number of retained Stodola/R-R modes.
p_ℓ , p_f , p_θ	number of retained Stodola/R-R modes for lead-lag, flap, torsion.

$\mathbf{q}$ — generalised coordinate vector in the aeroelastic formulation.

r^T — row vector relating θ_δ to $\mathbf{W}$.

s — spanwise variable.

$\hat{S}(\lambda)$ — matrix pencil - eqn (22).

$\bar{T}$ — transformation matrix - eqn (20).

$\upsilon(s\ ,\ t)$ — lead-lag displacement.

$\mathbf{V}$ — $= \{V_1(t)\ ,\ V_2(t)\ ,\ \ldots\}$, vector of lead-lag generalised coordinates.

$w(s\ ,\ t)$ — flap displacement.

$\mathbf{W}$ — $= \{W_1(t)\ ,\ W_2(t)\ ,\ \ldots\}$, vector of flap generalised coordinates.

$\mathbf{x}$ — eigenvector: basic Stodola mode formulation.

$\bar{\mathbf{x}}$ — $= \{\mathbf{V}\ ,\ \mathbf{W}\ ,\ \theta_p\ ,\ \boldsymbol{\theta}\}$

$\hat{\mathbf{x}}$ — $= \{\mathbf{V}\ ,\ \mathbf{W}\ ,\ \theta_0\ ,\ \boldsymbol{\theta}\}$ - eigenvector of rotational basis system.

$\mathbf{X}$ — modal matrix: basic Stodola mode formulation.

$\hat{\mathbf{X}}$ — modal matrix for rotational basis system.

$\bar{\mathbf{X}}$ — transformed modal matrix - eqn (28).

X_A — aerodynamic stiffness matrix.

Y_A — aerodynamic damping matrix.

$\Phi_j(\eta)$ — jth eigenfunction of uniform blade.

$\hat{\Phi}_j(\eta)$ — jth Stodola mode of non-rotating, non-uniform blade.

$\hat{\boldsymbol{\Phi}}$ — column vector of the $\hat{\Phi}_j$.

$\boldsymbol{\Phi}(s)$ — $= \{\Phi_V(s)\ ,\ \Phi_W(s)\ ,\ \Phi_\theta(s)\}$ normal mode set for the rotational basis system.

η — dimensionless spanwise variable.

$\theta(s\ ,\ t)$ — torsional variable.

$\theta_s(s)$ — pretwist function.

$\bar{\lambda}$ — eigenvalue of rotational basis system.

λ_j — jth aeroelastic eigenvalue.

$\theta_p(t)$ — pitch rotation.

$\theta_\delta(t)$ — pitch due to flap (δ_3)

$\theta_0(t)$ — pitch due to pcu flexibility.

$\boldsymbol{\theta}(t)$ — $= \{\theta_1(t)\ ,\ \theta_2(t)\ ,\ \ldots\ ,\}$, vector of torsional generalised coordinates.

Ω — rotation rate.

Introduction

In the modal analysis of highly non-uniform rotor blades, it is well known that the employment of assumed modes derived from the eigenfunctions of corresponding uniform blades is generally unsatisfactory; convergence properties are usually poor. It has been shown, (Ref 1), that if, instead, *smooth bending moment* (SBM) and *smooth torque* (ST) modes are employed, convergence properties are greatly improved. More recently, it has been shown, (Ref 2), that superior convergence characteristics are achieved when the assumed modes are generated by using one step of Stodola's method. Such modes are called Stodola modes. SMB and Stodola modes are generated with respect to the non-rotating, non-uniform blade, with no couplings between lead-lag, flap and torsional motions. A particular advantage of the Stodola mode formulation over the SBM method is that large inertia concentrations may be treated with more accuracy.

Stodola mode sets are usually highly ill-conditioned in the sense of poor orthogonality. In (Ref 1), this feature is removed by Rayleigh- Ritz (R-R) analysis, and a completely orthogonal set of 'Stodola/R-R' modes is thus obtained for the non-rotating blade. For blade bending it is shown that if only six Stodola modes are employed, the Stodola/R-R frequency spectrum comprises estimates of the first five non-rotating blade natural frequencies which are accurate to a small fraction of 1%.

The principal objective of the present paper is to describe the use of Stodola/R-R mode sets in the computer implementation of a rotor aeroelastic model, (Ref 3), which is to be used ultimately in flying qualities and active control research. We shall confine our attention to a LYNX-type metal blade and to the simple problem of hover trim and stability. The process of generation of the basic Stodola/R-R mode sets for the non-rotating blade will be reviewed and the generation of real, rotational, fully-coupled Stodola/R-R sets will be described and evaluated by recourse to a R-R sequence. The 'rotational basis system' with respect to which these rotational modes are calculated will comprise important subsidiary coupling effects associated with the pitch control linkage and power control units (pcu's). The rotational Stodola/R-R modes form our 'normal' mode set on which the aeroelastic analysis will be based. Aspects of hover trim, with the number of retained normal modes as a parameter, will be discussed and a final table of aeroelastic eigenvalues with respect to the hover configuration will be presented. Prediciton of blade bending moments will be briefly considered.

Generation of the Stodola/Rayleigh-Ritz Modes

We consider a hingeless rotor-blade of the LYNX genus. Typical variations of EI , GJ and m are shown in Fig 1. As comparison functions for flap, lead-lag and torsion, we choose sets of uniform, clamped-free beam eigenfunctions, $\phi_j(\eta)$, where η is the dimensionless spanwise variable and j runs from 1 to n . Bending is assumed to be sufficiently well described by the Euler-Bernoulli theory, so if $EI(\eta)$, $m(\eta)$ are the flexural rigidity (flapwise or lagwise) and mass/unit length functions for the actual blade, the first step in the formation of the jth Stodola mode is as follows:

Loading equation:

$$\mu_j(\eta) = \omega^2 m(\eta)\Phi_j(\eta) ; \qquad (1)$$

ω^2 set to unity.

Integrate for shear force:

$$S_j(\eta) = \ell\int_\eta^1 \mu_j(\eta)d\eta \qquad (2)$$

The backward integration is used because shear force is known to vanish at the tip. The remaining stages are as follows:

Integrate for bending moment:

$$M_j(\eta) = \ell\int_\eta^1 S_j(\eta)d\eta \qquad (3)$$

Determine curvature:

$$\hat{\Phi}_j''(\eta) = M_j(\eta)/EI(\eta) \qquad (4)$$

Integrate for slope:

$$\hat{\Phi}_j'(\eta) = \int_0^\eta \hat{\theta}_j''(\eta)d\eta \qquad (5)$$

Integrate for displacement:

$$\hat{\phi}_j(\eta) = \int_0^\eta \hat{\Phi}_j'(\eta)d\eta \qquad (6)$$

The jth Stodola mode is then $\hat{\Phi}_j(\eta)$: if EI is discontinuous, so also will be $\hat{\Phi}_j''$. But steps (5) and (6) ensure that $\hat{\Phi}_j$ is $C^{(1)}$ - continuous and therefore *admissible* for use in a Rayleigh-Ritz (R-R) analysis.

However, $\hat{\Phi}_j$ cannot be used in a Galerkin-type analysis, since the latter requires $C^{(2)}$ - continuity for the Euler-Bernoulli bending problem.

For torsion, the procedure is as follows:

Torsion loading equation:

$$\gamma_j(\eta) = m(\eta)k_p^2(\eta)\Phi_j(\eta) . \quad (7)$$

Integrate for local torque:

$$\tau_j(\eta) = \ell\int_\eta^1 \gamma_j(\eta)d\eta . \quad (8)$$

Determine torsional curvature:

$$\hat{\Phi}_j'(\eta) = \tau_j(\eta)/GJ(\eta) \quad (9)$$

Integrate for rotation:

$$\hat{\phi}_j(\eta) = \int_0^\eta \hat{\Phi}_j'(\eta)d\eta . \quad (10)$$

The jth Stodola torsion mode is then $\hat{\Phi}_j(\eta)$. If $GJ(\eta)$ is discontinuous, so also will be $\hat{\Phi}_j'$. But eqn (10) ensures that $\hat{\Phi}_j$ is $C^{(0)}$ - continuous and so is *admissible* for use in an R-R (but not Galerkin) analysis.

In obtaining the Stodola modes, we usually collocate at N spanwise stations, spaced in accordance with the variations of EI , GJ , m , k_p. The integration rule is arbitrary, but the writer's preference is for Simpson's first rule. In (Ref 2), this is shown to produce exceptional accuracy. For blade eigenanalysis, at a given level of accuracy, the use of trapezoidal-rule integration requires about three times the number of collocation points needed for Simpson's rule.

Stodola mode sets,

$\hat{\mathbf{\Phi}} = \{\hat{\Phi}_1 , \hat{\Phi}_2 , \ldots , \hat{\Phi}\}$, $n \ll N$ (usually), are in general not well conditioned - their orthogonality is poor. The writer prefers to confer orthogonality using a 'pre-processing' R-R analysis for the flap, lead-lag and torsion sets in isolation. (Note that flap/lag/torsion couplings are ignored in the formation of the Stodola modes. A coupled flap/lag version has been used, but this has little to commend it.) Thus for the flap set, for example, we form the eigenproblem, order n ,

$$\mathbf{E}\mathbf{x} = \lambda\mathbf{A}\mathbf{x} , \quad (11)$$

where

$$\mathbf{E} = (1/\ell^3)\int_0^1 EI_y(\eta)\hat{\mathbf{\Phi}}''(\eta)\hat{\mathbf{\Phi}}''^T(\eta)d\eta ,$$

$\mathbf{A} = \ell\int_0^1 m(\eta)\hat{\mathbf{\Phi}}(\eta)\hat{\mathbf{\Phi}}^T(\eta)d\eta$, and solve (by using a good pencil eigensolution technique) for $p \le n$ eigenvalue/vector pairs, λ_i , $\mathbf{x}_{(i)}$. The (n x p) modal matrix, $\mathbf{X} = [\mathbf{x}_{(1)} , \ldots , \mathbf{x}_{(p)}]$ may then be formed, where the modes $\mathbf{x}_{(i)}$ are arranged in ascending order of the λ_i. In obtaining eqn (11) we have used the modal expansion of the flap variable, viz

$$w(\eta , t) = \hat{\mathbf{\Phi}}^T(\eta)\mathbf{x}(t) , \quad (12)$$

and if now we write $\mathbf{x} = \mathbf{X}\mathbf{W}(t)$, then

$$w(\eta , t) = (\hat{\mathbf{\Phi}}^T\mathbf{X})\mathbf{W} \equiv \mathbf{F}^T\mathbf{W} . \quad (13)$$

Here, $\mathbf{W}$ is a set of p normal coordinates for flap *per se* and $\mathbf{F}(\eta)$ is a set of p Stodola/R-R modes. Similar sets, but perhaps with different numbers of members,

$$\upsilon(\eta , t) = \mathbf{f}^T(\eta)\mathbf{V}(t) ,$$

$$\theta(\eta , t) = \mathbf{h}^T(\eta)\mathbf{\theta}(t) , \quad (14)$$

are obtained for lead-lag and torsion respectively.

What we have achieved by using one stage of Stodola's method for each $\hat{\phi}_j$, coupled with R-R orthogonalisation, is an excellent approximation to what we would have achieved by using the *full* Stodola method, with successive re-orthogonalisation, (Ref 4), to calculate 'exact' **F**, **f** and **h** sets, but at a fraction of the cost.

The Rotational Basis System

Stodola/R-R modes are essentially real and are formed for a non-rotating blade, assuming no coupling between υ, w and θ. The next stage in the progression towards full aeroelastic implementation is to form a set of real, coupled, **F**, **f** and **h** modes for a steadily rotating blade with no aerodynamics. The writer assumes the blade to reside, at equilibrium, in the rotor plane. (No doubt, better ultimate results would be achieved if this basis system were appropriately coned-up and 'lagged'. But based on mass matrix orthogonality in subsequent aeroelastic studies, the use of the 'flat' basis configuration would appear to be sound.) Also, to keep the rotational modes real, all gyroscopic terms are ignored.

Albeit that the rotational basis system thus far described is simple, it is of vital importance that subsidiary structural effects which exert an influence on frequency spectrum should be included in it. For the LYNX-type blade under consideration, the most important subsidiary effect is that of swash-plate (dangle-berry) deflexion due to pcu flexibility. This leads to pitch becoming, in part, a generalised coordinate, which must therefore be appended to the torsional set, $\boldsymbol{\theta}$, of eqn (14). The δ_3-coupling effect would, of course, exist even if the pcu's and linkage were perfectly rigid - in which case, however, we would not need a pitch generalised coordinate. In general, all hinge effects need to be included in the rotational basis system. Some would contend that lag damper effects should also be included: this can be done, but the penalty is complex modes.

Into the energy expressions for our basis system we insert p_f, p_ℓ, p_t flap, lead-lag and torsion modes, together with a rigid-body pitch mode, $h_0(\eta)$, whose generalised coordinate is designated by $\theta_p(t)$. Let

$$\mathbf{x} = \{\mathbf{V}, \mathbf{W}, \theta_p, \boldsymbol{\theta}\},$$

$$\text{order } (\bar{n} \times 1);$$

$$\bar{n} = p_f + p_\ell + p_t + 1, \qquad (15)$$

be the composite vector of the generalised coordinates of the basis system. Then the conservative eigenproblem posed by this system is

$$(\bar{\mathbf{E}} + \Omega^2\bar{\mathbf{C}})\bar{\mathbf{x}} = \bar{\lambda}\,\bar{\mathbf{A}}\,\bar{\mathbf{x}}. \qquad (16)$$

In the formulation of (Ref 3), each of the square matrices appearing in eqn (16) is fully coupled. If Stodola/R-R modal sets are employed, the 'VV', 'WW', 'θθ' submatrices of $\bar{\mathbf{E}}$ and $\bar{\mathbf{A}}$ become diagonal, but no computational advantages accrue from these special forms. If, as in (Ref 1), θ_p is taken as the *total* pitch rotation due to pcu flexibility and the δ_3-coupling effect of the pitch-control linkage, strong off-diagonal terms occur in the 'WW', '$W\theta_p$', 'θ_pW' submatrices of $\bar{\mathbf{E}}$, these terms being proportional to k, the pcu effective stiffness. When k is large, certain methods for eigenanalysis of eqn (16) fail due to numerical ill-conditioning. In order to avert such problems, the writer uses the relationship

$$\theta_p = \theta_\delta + \theta_0 \qquad (17)$$

where θ_δ is the 'δ_3' pitch and θ_0 is the pitch due to pcu flexibility. It is then easy to show that

$$\bar{x} = \bar{T}\hat{x} \qquad (18)$$

where

$$\hat{x} = \{V, W, \theta_0, \theta\} \qquad (19)$$

$$\text{and } \bar{T} = \begin{bmatrix} I & 0 & 0 & 0 \\ 0 & I & 0 & 0 \\ 0 & r^T & 1 & 0 \\ 0 & 0 & 0 & I \end{bmatrix} \qquad (20)$$

It is evident that $\theta_\delta = r^T W$, and that if eqn (18) is used to transform eqn (16) congruently to yield

$$(\hat{E} + \Omega^2\hat{C})\hat{x} = \bar{\lambda}\,\hat{A}\,\hat{x}\,, \qquad (21)$$

where $\hat{E} = \bar{T}^T\bar{E}\bar{T}$, etc, then the effects of θ_δ are implicit in the inertia matrices $\hat{A}$ and $\hat{C}$, while being absent from $\hat{E}$. The net result is that the θ_0 row and column of $\hat{E}$ are null, except for ka^2 in the diagonal position, 'a' being the effective operating radius of the pitch-control linkage. The above mentioned numerical problems associated with large k are therefore removed and the δ_3-coupling effects are accorded their logical roles in the inertia (and later, aerodynamic) matrices.

Use of the formation based on eqn (21) enables cases in which k is very large (ie pcu's with very large real impedance) to be dealt with simply by deleting the θ_0-rows and columns of E, C, etc, and by removal of θ_0 from the generalised coordinate vector, $\hat{x}$. Such an expedient cannot be used in the formulation based on eqn (16).

Eigensolution of eqn (21) is accomplished by use of a fully pivotal version of the Newtonian technique described in (Ref 5). This technique is applicable since the matrix pencil

$$\hat{S}(\bar{\lambda}) = \hat{E} + \Omega^2\hat{C} - \bar{\lambda}\hat{A} \qquad (22)$$

is regular, symmetric and real.

Solution pairs $\bar{\lambda}_i$, $\hat{x}_i$ are obtained, in strict ascending order of the $\bar{\lambda}_i$, over a stated eigenvalue range, and with the certainty that none has been missed. The $\hat{x}_i$ are normalised automatically in accordance with

$$\hat{x}_i^T\hat{A}\hat{x}_i = 1 \qquad (23)$$

so that

$$\hat{x}_i^T(\hat{E} + \Omega^2\hat{A})\hat{x}_i = \bar{\lambda}_i \qquad (24)$$

The number, m, of solution pairs retained for subsequent aeroelastic analysis is determined by the required bandwidth. Modal and spectral matrices

$$\hat{X} = [\hat{x}_1, \hat{x}_2, \ldots, \hat{x}_m]\,,$$
$$\hat{\Lambda} = \text{diag}\,[\bar{\lambda}_1, \bar{\lambda}_2, \ldots, \bar{\lambda}_m] \qquad (25)$$

are then formed. In view of eqn (23) and eqn (24), we have

$$\hat{X}^T\hat{A}\hat{X} = I\,, \quad \hat{X}^T(\hat{E} + \Omega^2\hat{C})\hat{X} = \hat{\Lambda} \qquad (26)$$

With the $(\bar{n} \times m)$ modal matrix partitioned in the form

$$\hat{X} = \begin{bmatrix} X_v \\ X_w \\ x_0^T \\ X_0 \end{bmatrix} \begin{array}{l} \leftarrow p_\ell \text{ rows} \\ \leftarrow p_f \text{ rows} \\ \leftarrow 1 \text{ row} \\ \leftarrow p_t \text{ rows} \end{array} \qquad (27)$$

eqns (18)-(20) yield the resolved modal matrix

$$\bar{X} = \bar{T}\hat{X} = \begin{bmatrix} X_v \\ X_w \\ x_0^T + r^T X_w \\ X_0 \end{bmatrix} \qquad (28)$$

Thus, if $q = \{q_1 , q_2 , \dots , q_m\} \equiv q(t)$ is the *normal* coordinate vector of the rotational basis system, the physical variables $\upsilon(s , t)$, $\omega(s , t)$, $\theta(s , t)$ are related to the normal coordinates, $q_j(t)$, by

$$\begin{bmatrix} \upsilon(s , t) \\ \omega(s , t) \\ \theta(s , t) \end{bmatrix} = \begin{bmatrix} f^T(s)X_v \\ F^T(s)X_w \\ h_0(s)(x_0^T + r^T X_w) + h^T(s)X_0 \end{bmatrix} q(t) \equiv \begin{bmatrix} \Phi_v(s) \\ \Phi_w(s) \\ \Phi_\theta(s) \end{bmatrix} q(t) \equiv \Phi(s)q(t) \qquad (29)$$

The normal mode set, $\Phi(s)$, is stored in partitioned numerical form as $\Phi_v(s_k)$, $\Phi_w(s_k)$, $\Phi_\theta(s_k)$; $k = 0 , 1 , 2 , \dots , N$, for subsequent use in the aeroelastic analysis. Slopes and curvatures must also be similarly stored.

Aeroelastic Analysis

The theory provided in (Ref 3) for individual blade aeroelasticity is quite standard in that it reflects the previous theories of Houbolt and Brooks (Ref 6), Hodges and Dowell (Ref 7), and others. It is distinguished from the previous theories by (i), the *ab initio* inclusion of shaft flexibility effects, (ii), the use of branch modes philosophy and (iii), the full development (by longhand methods) of all terms in the modal Lagrangian equations of motion so as to embrace every conceivable manoeuvre state of the rotorcraft. The aerodynamic description used in (Ref 3), however, is 'simple' in that it is based on tailored strip theory, albeit that Prandtl-Glauert compressibility correction of all circulatory aerodynamic derivatives is included and unsteady effects are allowed for. For the flying qualities applications at which the model is aimed, it is planned to incorporate the Pitt and Peters dynamic inflow description (Ref 8), table look-up sectional aerodynamics and limited wake model-ling in order to represent blade/vortex interactions. (Ref 3) provides a complete set of linear equations of motion with respect to an equilibrium configuration in the rotor plane. Important elastic and inertial nonlinear effects, of quadratic and cubic order of blade slopes, are included in order to enable (amongst other things) linearisation with respect to coned-up/lagged equilib-rium configurations. Indeed, the writer has developed full expressions, in modal form, for *all* quadratic and many cubic nonlinear effects. With regard to general solution techniques, a perturbational Floquet theory has been written in extended form (up to the second order of the perturbation parameter) for application to the modal equations of motion in multi-blade co-ordinate form: this is to be used in the *stability analysis code* on which the writer is currently working. Work is to begin shortly on the *numerical integration code* which will be used in the context of performance in manoeuvres: ultimately this code will be required to run in real time for simulation applications. The rotational Stodola/R-R modal set, eqn (29), will be used as the basis of the foregoing applications, as well as in the RAE LYNX Modelling validation exercise wherein comparisons with measured blade strains will be made.

In this paper, our attention will be confined to the simple hover state in which the rotor has to balance only a vertical load and, of course, the torque provided by the engines. The shaft will therefore twist, but not flex and may sensibly be regarded as rigid. Simple aerodynamics will be used, allied with the Glauert inflow description. Iteration is required in order to progress from the initial 'flat' rotor configuration to the coned-up/lagged hover equilibrium state. At each stage of the iteration, the elastic, centrifugal and aerodynamic stiffness matrices, along with all terms on the RHS of Lagrange's equations are fully updated in respect of the current state of twist/pitch and nonlinear effects associated with flap-up and lag. Convergence to hover equilibrium is quadratic and between four and six iterations are usually required. The number, m, of rotational Stodola/R-R modes (eqn (29)) required to represent adequately the equilibrium state of the typical blade varies between five and fifteen, dependent on the position in the basic frequency spectrum of the fundamental torsion-dominant mode, and on the extent of pre-cone, pre-lead and foward offset of the blade.

When convergence to equilibrium has been achieved, the stability of equilibrium is assessed by solution of

$$\mathbf{A}\ddot{\mathbf{q}} + (\mathbf{D} + \mathbf{Y}_A + \Omega\mathbf{B})\dot{\mathbf{q}} + (\mathbf{E} + \mathbf{X}_A + \Omega^2\mathbf{C})\mathbf{q} = \mathbf{0}\ , \qquad (30)$$

where, with suffixes, circumflexes and overbars omitted for convenience,

A is the symmetric, classical, inertia matrix,

D is the symmetric lag/ structural damping matrix,

$\mathbf{Y}_A$ is the aerodynamic damping matrix,

$\Omega\mathbf{B}$ is the skew-symmetric gyroscopic matrix,

E is the elastic stiffness matrix,

$\mathbf{X}_A$ is the aerodynamic stiffness matrix, and

$\Omega^2\mathbf{C}$ is the centrifugal stiffness matrix,

all of which are of order m and are evaluated with respect to the coned-up/lagged equilibrium configuration. Eigensolution, which is effectively a further generalised R-R analysis, is accomplished in the stability code by use of the writer's specially tailored version of the QR and inverse iteration algorithms. No library program calls are required.

Notes on Spanwise Integration Involving Stodola Modes and B.M. Prediction

In order to extract the maximum benefit from Stodola modes, it is necessary to represent every discontinuity of EI, GJ, etc, (and hence of every Stodola mode), precisely. Thus, every set of numbers representing EI, GJ, etc, and any Stodola mode, must be accompanied by another (shorter) set of numbers representing the 'jumps' in these functions. Again, when using Simpson's rule, the number of intervals across the blade span, ℓ, is even, ie $N = 2N_s$, say, and while the N_S 'double intervals' may be of unequal length, the two sub-intervals of each double-interval must be of equal length. This restriction may be removed by use of an 'unequal interval' version of Simpson's rule. However, the multiplication count of the latter is, at best, 2.4 times that of the simple 'first rule'.

For the present blade, N = 60 is used and there are nine 'jumps'. But for aerodynamic force/moment evaluations, we sub-collocate to $N_A = 18$ station points with no 'jumps'. The choice of N = 60 for the blade structural actions facilitates accurate calculation of bending moments and torques at selected points across the span. This is demonstrated in Table 1 for uncoupled steady flap (cone-up) of the blade under aerodynamic loading with parabolic spanwise distribution, with $\Omega = 35$ rad/s. The numerical integration results were obtained by using 25 Stodola/R-R flap modes -for which number the bending moment distribution had sensibly converged. The 'M = EIw"' results were obtained by using 10 non-rotating Stodola/R-R modes in the rotational basis system formulation: the first four modes of the rotational system were then used to evaluate the bending moments. In brackets in the final column are the percentage bending moment errors when the first four rotational modes are based on 18 non-rotating modes. Contraflexure near the tip owing to the centrifugal actions on the concentrated mass at 95-98% span cannot be represented by four modes -hence the large percentage errors in the (small) bending moments at and beyond 90% span. All nine jumps are covered in Table 1, thus lending confidence to the internal load prediction capability of the Stodola/R-R modes.

Numerical shake tests at frequencies up to 45 Hz using lift distributions of the form

$$L(s) \; \alpha \; \left(\frac{s}{\ell}\right)^2 \sin \frac{(2p-1)\pi\eta}{2} \; \exp(i\omega_f t) \tag{31}$$

with integer p appropriately related to forcing frequency, ω_f, have also been undertaken. Excellent bending moment predictions resulted, even with only four retained modes, as above. For excitation frequencies greater than 45 Hz (which is between the frequencies of flap modes 4 and 5), more retained modes are obviously required. The static results presented in Table 1 are, in fact, close to the worst, *vis a vis* B.M. prediction. For as ω_f increases from zero, deleterious effects, such as contraflexure near the tip, are 'shaken-out' and results become uniformly good across the entire span.

Convergence of Initial, Non-Rotational, Flap, Lead/Lag and Torsional Stodola/R-R Sequences

This topic has been covered *in extenso*, for hypothetical rotor blades in Ref 2. It is shown that with only six Stodola modes, the first five natural frequencies in each uncoupled, non-rotational set (ie lead-lag, flap and torsion) are predicted to within 0.5%. Similar, excellent, convergence properties obtain for the blade of Fig 1. It is felt not to be necessary to present the R-R sequences herein: the first ten lead/lag, flap and torsional uncoupled, non-rotating natural frequencies for $p_\ell = p_f = p_t = 15$ are given in Table 2.

Convergence of the Coupled Lead/Lag, Flap, Pitch and Torsion Modes of the Rotational Basis System

The pre-processing program, 'SRMODES' which generates the non-rotational Stodola/R-R modes, produces data files 'LAG.DAT', 'FLAP.DAT' and 'TOR.DAT' containing the lead-lag, flap and torsion modes. 'SRMODES' is fed by the basic blade data file 'SR.DAT'. The pre-processing program 'SROT', which generates the rotational basis system normal modes, is fed by all four data files above, and produces output files 'SRO.DAT' and 'ROT.DAT'. 'SRO.DAT' comprises a scaled version of 'SR.DAT', while 'ROT.DAT' contains the normal mode set $\Phi(s)$, $\Phi'(s)$, $\Phi''(s)$ -eqn (29). These data files feed the aeroelastics code, 'ZHOVER'. The pre-processing programs enable the setting of a reference pitch angle, θ_R, upon which all derived sectional properties of the blade are based (along with the pre-twist setting $\theta_S(s)$).

Our test blade has a washout, from root setting zero, of 0.1 rad. In the following convergence studies, $\theta_R = 0.2$ rad is used. The pitch control linkage geometry is as per LYNX, but the pcu effective stiffness $k = 2.1 \times 10^6$ N/m, has been set lower than the LYNX value in order to place the pitch-dominant mode in the fourth position in the rotational frequency spectrum - as in Ref 1. This adjustment is necessary because our test blade is 'pseudo-LYNX' rather than actual LYNX. Rotation rate is set at $\Omega = 34.17$ rad/s.

Of the 15 non-rotating Stodola/R-R modes, 10 lead-lag, 10 flap and 9 torsion modes are used as input to the rotation modes program 'SROT'. With the single pitch mode added, this gives 30 input modes - the maximum number for the present version of the 'SROT' code. The maximum number of rotational, normal, output modes is nine. For the test blade, these modes are as follows:

<u>Mode 1</u>: Lead-lag 1.
<u>Mode 2</u>: Flap 1.
<u>Mode 3</u>: Flap 2 - Pitch.
<u>Mode 4</u>: Pitch - Torsion 1.
<u>Mode 5</u>: Lag 2.
<u>Mode 6</u>: Flap 3.
<u>Mode 7</u>: Pitch - Flap 4.
<u>Mode 8</u>: Torsion 1 - Pitch.
<u>Mode 9</u>: Torsion 1 - Lag 3 - Pitch.

All normal modes are, of course, fully coupled. Important interactions only are indicated above. Table 3 gives the Rayleigh-Ritz sequence for the rotational basis system of our test blade in terms of natural frequencies (Hz) when $p_\ell = p_f = p_t = j$; $j = 1, 2, \ldots, 9$. The final row of the table applies to $p_\ell = p_f = 10$, $p_t = 9$; this is the case which is carried forward into the aeroelastic program, 'ZHOVER'. The Rayleigh-Ritz sequence exhibits impressive convergence properties. [Note that placements in the table for Modes 7-9 when $j \leq 3$ are based on the 'decreasing frequency for increasing j' logic of Rayleigh-Ritz sequences, rather than on classification by mode shape.] It is clear that adoption of $j = 5$ (giving 16 input modes) would lead to a maximum error of about 0.5% over the whole set of nine rotational natural frequencies. With $j = 4$ (13 input modes), the corresponding maximum error would be about 1.5%.

<u>Hover Equilibrium: Aeroelastic Eigenvalues</u>

The test blade is assumed to be the 'typical blade' of a four-blade ($n_B = 4$), LYNX-type rotor. It has a constant precone angle of about 1½° and the droop angle is zero. There is no pre-lead angle, but the blade root has a forward offset, $\bar{Y}_0 = 25$ mm, as on the LYNX blade. In the hover condition, the disc loading is assumed to be 40 kN. Unless otherwise stated, the aerodynamic coefficients are those for an NPL 9615 aerofoil with no compressibility corrections. There is no blending of aerofoil sections across the span.

Lag damping is set untypically low at about 2% of critical in the Lag 1 mode. This has been done so as not to 'pollute' the aeroelastic eigenvalues with large real parts and corresponding frequency shifts.

Structural damping is ignored; all other damping is therefore of aerodynamic origin.

Fig 2 shows lead-lag and flap deflexions and total flap displacement (including pre-cone) from the rotor plane. The parameter is m, the number of retained rotational Stodola/R-R modes. For $m \geq 5$, the curves of Fig 2 do not change, to visible extent, with m, but for $m = 4$, lead-lag deflexion is seen to be extremely poorly predicted. This is because only one of the retained modes, viz Mode 1, has a significant lead-lag content - this being the fundamental lag mode. But the deflected shape to be represented has a strong 'Lag 2' content, and only when m is increased to 5 does this mode appear.

Fig 3 shows the lead-lag and flap bending moments for the test blade in the hover condition. The variability of the bending moments with m is large, as might have been expected - especially for the smaller values of m. For $m = 8$, the values are shown on the graphs owing to the fact that the flap values are indistinguishable from those for $m = 9$, while the lead-lag values are virtually identical to those for $m = 6$. (NB, Mode 9 has strong 'Lag 3' content). The bending moments were obtained by using the constitutive relationships for the blade.

An important feature of the Stodola mode description, which is shared by the SBM mode approach of Ref 1, is the 'smoothness' ($C^{(0)}$ continuity) of the bending moment functions. The associated curvatures, of course, are highly discontinuous. Now our Stodola flap modes, for example, are based on

$$EI_y = EI_{FLAT} \cos^2\bar{\theta}_R + EI_{EDGE} \sin^2\bar{\theta}_R \,, \qquad (32)$$

where $\bar{\theta}_R$ is the reference orientation of the blade at s. Thus $EI_y F''$ is a vector of continuous functions. But when, during iteration to the equilibrium state, $\bar{\theta}_R$ varies due to blade twist and control pitch, EI_y is changed in accordance with eqn (32), so that $EI_y F''$ is no longer continuous - except in regions of 'matched stiffness' ($EI_{FLAT} = EI_{EDGE}$). For this reason, $\bar{\theta}_R$ should be set as closely as possible to its final converged, average, value when using Stodola modes in the load-prediction context. The bending moment discontinuities are not evident in Fig 3 because of the smallness of the changes in the original blade setting.

Table 4 relates to aeroelastic stability in the hover condition. In each case, the hover equilibrium state was determined using the same number, m, of modes used in the subsequent stability analysis. The trim cases are detailed in Table 4(a). Here, θ_{tip} includes elastic twist, washout, quasi-twist and total collective, while total collective includes the initial reference setting, trim collective, δ_3 pitch and pitch due to pcu flexibility. M_{fh} is the total pitching moment about the feathering hinge. The table shows that blade geometry at hover may be described accurately by using only five modes. Two additional $m = 9$ cases have been included, both with Prandtl-Glauert compressibility correction, the second with doubled rotor thrust.

The aeroelastic eigenvalues for each of the cases encompassed by Table 4(a) are given in Table 4(b). The matrices which form the basis of this table (c.f. eqn (30)) are exemplified for $m = 6$:

Total Stiffness Matrix, $(\mathbf{E} + \mathbf{C} + \mathbf{X}_A)/1000$

$$\begin{bmatrix} 0.471 & -0.033 & -0.305 & 2.613 & -0.100 & 0.075 \\ -0.032 & 1.787 & 3.399 & -29.119 & 1.146 & -0.882 \\ -0.001 & 0.024 & 9.614 & -2.526 & 0.148 & -0.296 \\ -0.004 & -0.026 & -0.986 & 16.713 & -0.658 & -1.017 \\ -0.001 & 0.024 & 0.143 & -2.031 & 28.390 & -0.187 \\ 0.007 & -0.096 & -0.943 & 7.352 & -0.450 & 34.655 \end{bmatrix}$$

Total Damping Matrix, $\mathbf{D} + \mathbf{B} + \mathbf{Y}_A$

$$\begin{bmatrix} 0.750 & -4.356 & -0.682 & -0.992 & -4.580 & 2.775 \\ 5.804 & 28.862 & 0.703 & 0.675 & 0.464 & -8.918 \\ 1.483 & 1.486 & 19.439 & -3.629 & 7.306 & 6.759 \\ 1.476 & -0.386 & -6.518 & 53.933 & -1.440 & 1.376 \\ 2.150 & 0.634 & -3.061 & -2.700 & 2.592 & -1.507 \\ -3.257 & -8.299 & 5.236 & 0.603 & 1.698 & 18.962 \end{bmatrix}$$

Classical Inertia Matrix, $\mathbf{A}$

$$\begin{bmatrix} 1.000 & -0.001 & 0.000 & 0.000 & 0.000 & 0.000 \\ -0.001 & 1.003 & 0.001 & 0.000 & -0.001 & -0.003 \\ 0.000 & 0.001 & 1.003 & 0.000 & -0.001 & 0.000 \\ 0.000 & 0.000 & 0.000 & 1.000 & 0.001 & 0.000 \\ 0.000 & -0.001 & -0.001 & 0.001 & 1.000 & -0.001 \\ 0.000 & -0.003 & 0.000 & 0.000 & -0.001 & 1.005 \end{bmatrix}$$

*** NB The above matrices contain the linearised effects of important non-linear terms ***

Note the $\mathbf{C}$ and $\mathbf{B}$ now include Ω^2 and Ω respectively. The $\mathbf{q}$ vector of (30) comprises the generalised co-ordinates of Mode 1, Mode 2, etc, in turn.

Little can be said about the contents of Table 4(b). It exhibits remarkable consistency throughout, even for $m = 4$. The lag-dominant modes are those associated with λ_1, λ_5 and λ_9; all have low 'PCD's' owing to the smallness of the lag damping. The general effect of the compressibility correction is to increase the 'PCD's' and concomitantly to reduce the 'UNF's'. As expected, all modes for all values of m are thoroughly stable.

Conclusions

The various stages of application of the Stodola/R-R mode technique (Ref 2) to rotor aeroelastic problems have been described, and exemplified for the simple case of hover equilibrium. A Rayleigh-Ritz sequence for rotational Stodola/R-R modes has been presented, and although the convergence properties of this sequence are not so dramatic as in the non-rotational case (Ref 2), they are nevertheless very good. While blade geometry in the hover condition may be described by using a small number of rotational Stodola/R-R modes, it has been shown that many more modes may need to be added in order to facilitate accurate prediction of blade strains.

For the principal application of this aeroelastic analysis, in real-time simulation to establish performance benefits and constraints on the application of ACT, it is expected that the first few modes will be adequate. This research is continuing toward this application with more general trim states and large amplitude manoeuvres.

References

1 DONE, G. T. S. & PATEL, M. H. 1988. "The use of smooth bending moment modes in helicopter rotor blade vibration studies." Journal of Sound & Vibration 123(1), 71-80.

2 SIMPSON, A. 1989. "On the generation of a set of accurate numerical modal functions for use in the aeroelastic analysis of flexible rotor blades." The Aeronautical Journal, June-July 1989, 207-218.

3 SIMPSON, A. 1988. "Derivation of modal Langrangian equations of motion for a multi-blade flexible rotor on a flexible shaft." University of Bristol Contract Report AS3/88." SERC/MOD Contract XG11814. (In preparation as an RAE TR).

4 DEN HARTOG, J. P. 1947. "Mechanical Vibrations," 3rd ed., McGraw-Hill.

5 SIMPSON, A. 1984. " Newtonian procedure for the solution of $S(\lambda)x = 0$." Journal of Sound & Vibration 97(1), 153-164.

6 HOUBOLT, J. C. & BROOKS, G. W. 1958. "Differential equations of motion for combined flapwise bending, chordwise bending, and torsion of twisted nonuniform rotor blades." NACA Report No 1346.

7 HODGES, D. H. & DOWELL, E. H. 1974. "Nonlinear equations of motion for the elastic bending and torsion of twisted nonuniform rotor blades." NASA TN D-7818.

8 PITT, D. H. & PETERS, D. A. 1981. "Theoretical prediction of dynamic inflow derivatives." Vertica, 5, 21-34.

TABLE 1

Comparison of uncoupled flap BMs evaluated by M = EIw'' for four rotational Stodola/R-R modes (obtained using ten non-rotating Stodola/R-R modes) with BMs from numerical integration of aerodynamic and inertia forces: Ω = 35 rad/s , lift $\alpha\ s^2/\ell^2$

η (% span)	w (m)	10w' (rad x 10)	100w'' (rad/m x 100)	100w'' jump (rad/ m x 100)	EI w'' (Nm)	BM INT (Nm)	BM Error (%)
1	0.0000	0.023	8.878	0.000	5176	5419	-4.5(-1.7)
5	0.0039	0.320	12.606	0.000	3782	3673	3.0(0.1)
6	0.0060	0.370	5.745	1.379	3447	3417	0.9(-2.2)
8	0.0105	0.385	1.141	5.703	2852	2947	-3.2(-2.6)
10	0.0155	0.448	4.769	0.822	2385	2531	-5.8(-0.5)
12	0.0210	0.458	0.824	2.745	2059	2152	-4.3(0.3)
20	0.0492	0.656	0.456	0.000	1301	1363	-4.5(-2.9)
26	0.0740	0.720	1.641	1.970	985	980	0.5(-0.6)
40	0.1405	0.859	1.525	0.000	656	637	3.0(-0.3)
52.5	0.2092	0.970	1.423	1.851	555	558	-0.5(-1.8)
66	0.2869	1.099	1.605	2.043	450	460	-2.2(-3.0)
75	0.3564	1.214	1.689	0.000	321	334	-3.9(-3.9)
80	0.3936	1.262	1.391	0.000	250	243	2.9(4.1)
90	0.4714	1.323	0.591	0.000	83	42	97.6(114.3)
95	0.5113	1.335	0.177	0.026	19	-7	371(34)
98	0.5273	1.335	0.008	0.051	6	-10	160(110)
100	0.5513	1.336	0.000	0.000	0	0	0(0)

NB Bracketed percentages relate to the case of 18 non-rotational modes.

TABLE 2

Natural frequencies of the Stodola/R-R non-rotational, uncoupled, modes for the test blade (Hz)

Mode Number	Lead/Lag	Flap	Torsion
1	2.5103	1.6518	35.7974
2	23.9098	8.4557	90.0283
3	63.0654	22.380	164.866
4	111.821	41.2110	232.245
5	193.751	68.0865	299.266
6	274.609	105.768	375.975
7	375.394	150.280	437.042
8	507.162	201.219	488.522
9	634.538	256.871	567.720
10	812.532	323.787	646.232

TABLE 3

Rayleigh-Ritz sequence for rotational basis system natural frequencies (Hz) of the test blade ($p_\ell = p_f = p_t = j\epsilon(1,9)$, Ω = 34.17 rad/s)

j	Mode 1	Mode 2	Mode 3	Mode 4	Mode 5	Mode 6	Mode 7	Mode 8	Mode 9
1	3.4841	6.1805	-	21.6934	-	-	59.4734	-	-
2	3.4711	6.0368	15.4710	21.6658	26.8664	-	53.7009	>71.2	-
3	3.4551	6.0023	15.3525	21.6197	26.8477	30.2499	53.6500	65.3744	>71.2
4	3.4481	5.9947	15.3273	21.5771	26.7728	29.7698	49.3983	53.6737	65.4655
5	3.4457	5.9929	15.3266	21.5096	26.7604	29.7305	48.7118	53.1903	64.8706
6	3.4450	5.9927	15.3249	21.4852	26.7574	29.7222	48.7099	53.1298	64.7583
7	3.4449	5.9924	15.3238	21.4494	26.7563	29.6960	48.6557	53.0052	64.7304
8	3.4448	5.9923	15.3237	21.4325	26.7555	29.6898	48.6343	52.9931	64.7142
9	3.4446	5.9922	15.3228	21.4036	26.7546	29.6772	48.6304	52.9036	64.6939
10*	3.4445	5.9921	15.3222	21.3806	26.7539	29.6641	48.6129	52.8913	64.6799

NB * $p_\ell = p_f = 10$, $p_t = 9$

TABLE 4

Test-blade stability in the hover equilibrium condition; Ω = 34.17 rad/s:

(a) Details of trim cases for various m values

m	v_{tip} (mm)	w_{tip} (mm)	θ_{tip} (deg)	Total Collective (deg)	M_{fh} (Nm)	Thrust KN	Power KW
4	-37.2	343.6	4.56	13.29	-525.8	40	583.9
5	-53.7	343.3	4.61	13.23	-511.1	40	583.9
6	-53.7	343.9	4.62	13.22	-507.8	40	583.9
7	-53.2	341.6	4.56	13.16	-467.6	40	583.6
8	-53.2	342.1	4.59	13.15	-475.5	40	583.7
9	-54.1	342.3	4.61	13.15	-487.8	40	583.7
9*	-59.4	350.7	3.74	12.52	-524.6	40	606.3
9#	-215.9	723.1	8.87	19.63	-842.5	80	1480.0

NB * Prandtl-Glauert compressibility corrected values.
Prandtl-Glauert compressibility corrected values at double thrust.

(b) Aeroelastic eigenvalues

m		λ_1	λ_2	λ_3	λ_4	λ_5	λ_6	λ_7	λ_8	λ_9
4	PCD	1.827	31.516	9.668	21.725	-	-	-	-	-
	UNF	3.419	6.465	15.316	20.149	-	-	-	-	-
5	PCD	1.892	32.754	9.497	21.245	0.9773	-	-	-	-
	UNF	3.412	6.311	15.221	20.337	26.844	-	-	-	-
6	PCD	1.909	32.066	9.588	21.475	0.9434	4.909	-	-	-
	UNF	3.413	6.317	15.236	20.556	26.839	29.317	-	-	-
7	PCD	1.925	32.343	9.586	21.702	0.9426	4.980	3.161	-	-
	UNF	3.413	6.321	15.246	20.475	26.838	29.350	48.183	-	-
8	PCD	1.926	32.441	9.432	21.725	0.9405	4.967	3.201	4.637	-
	UNF	3.413	6.328	15.290	20.496	26.836	29.337	48.262	53.000	-
9	PCD	1.910	32.184	9.459	21.804	0.9423	4.859	3.235	4.643	0.6307
	UNF	3.414	6.333	15.276	20.640	26.838	29.275	48.273	52.969	64.636
=====		======	=======	=======	=======	========	=======	=======	=======	=======
9*	PCD	2.213	39.814	11.147	27.316	0.9211	5.767	3.905	5.774	0.6517
	UNF	3.410	6.303	15.196	20.395	26.842	29.204	48.213	52.966	64.683
9#	PCD	5.282	37.577	11.108	27.292	0.8963	5.515	3.682	5.773	0.8923
	UNF	3.306	6.400	15.070	20.783	26.593	29.266	48.481	52.926	64.170

PCD - Percentage of critical damping
UNF - Undamped natural frequency (Hz)-effective

NB * Prandtl-Glauert compressibility corrected values.
Prandtl-Glauert compressibility corrected values at double thrust.

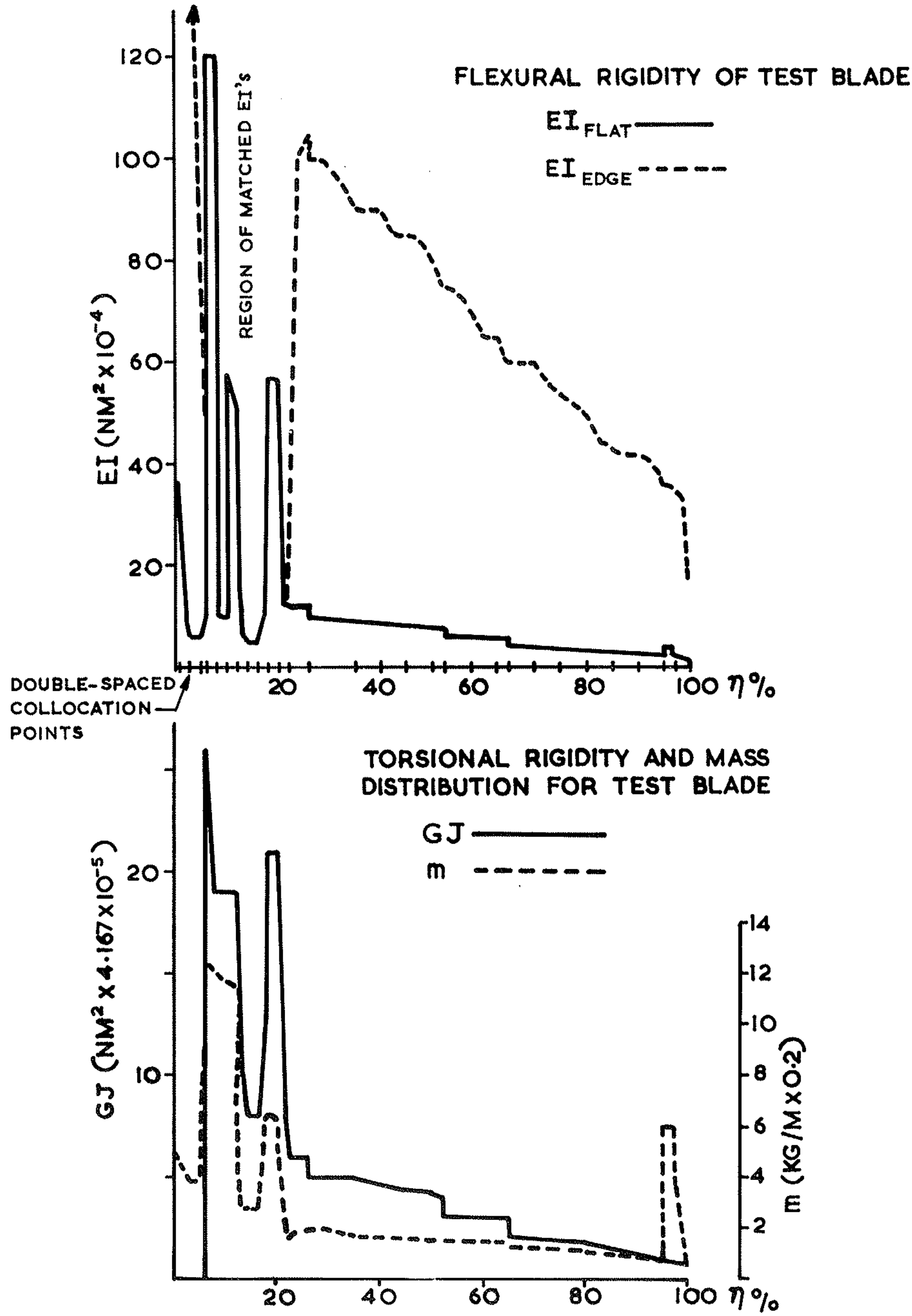

FIG. 1 SELECTED SECTION PROPERTIES OF THE TEST BLADE

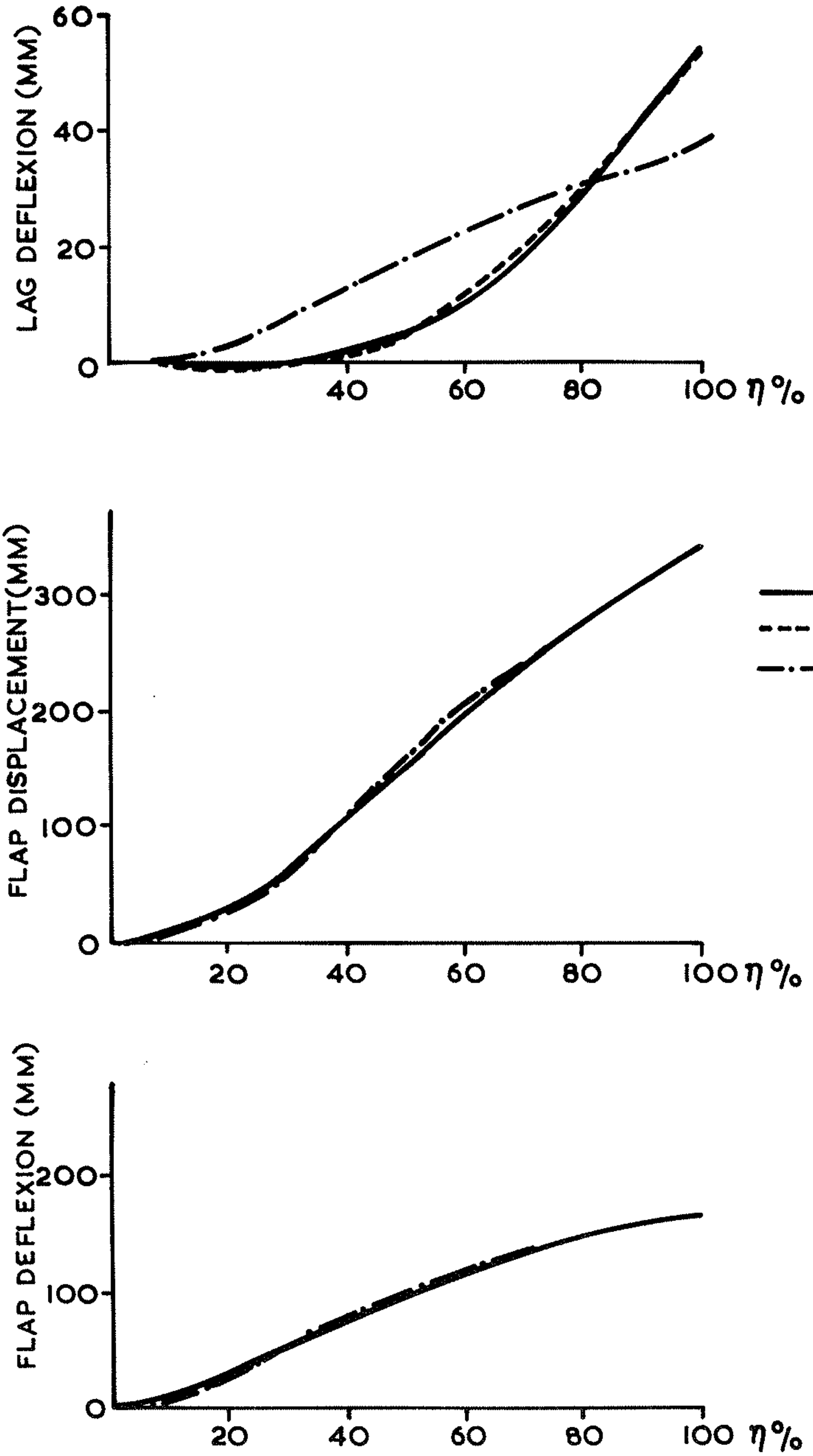

FIG.2 DEFLEXIONS/DISPLACEMENTS OF BLADE IN HOVER EQUILIBRIUM WITH NUMBER OF RETAINED MODES AS THE PARAMETER (DISC LOADING = 40 KN, NB=4, Ω=34.17 RAD/S)

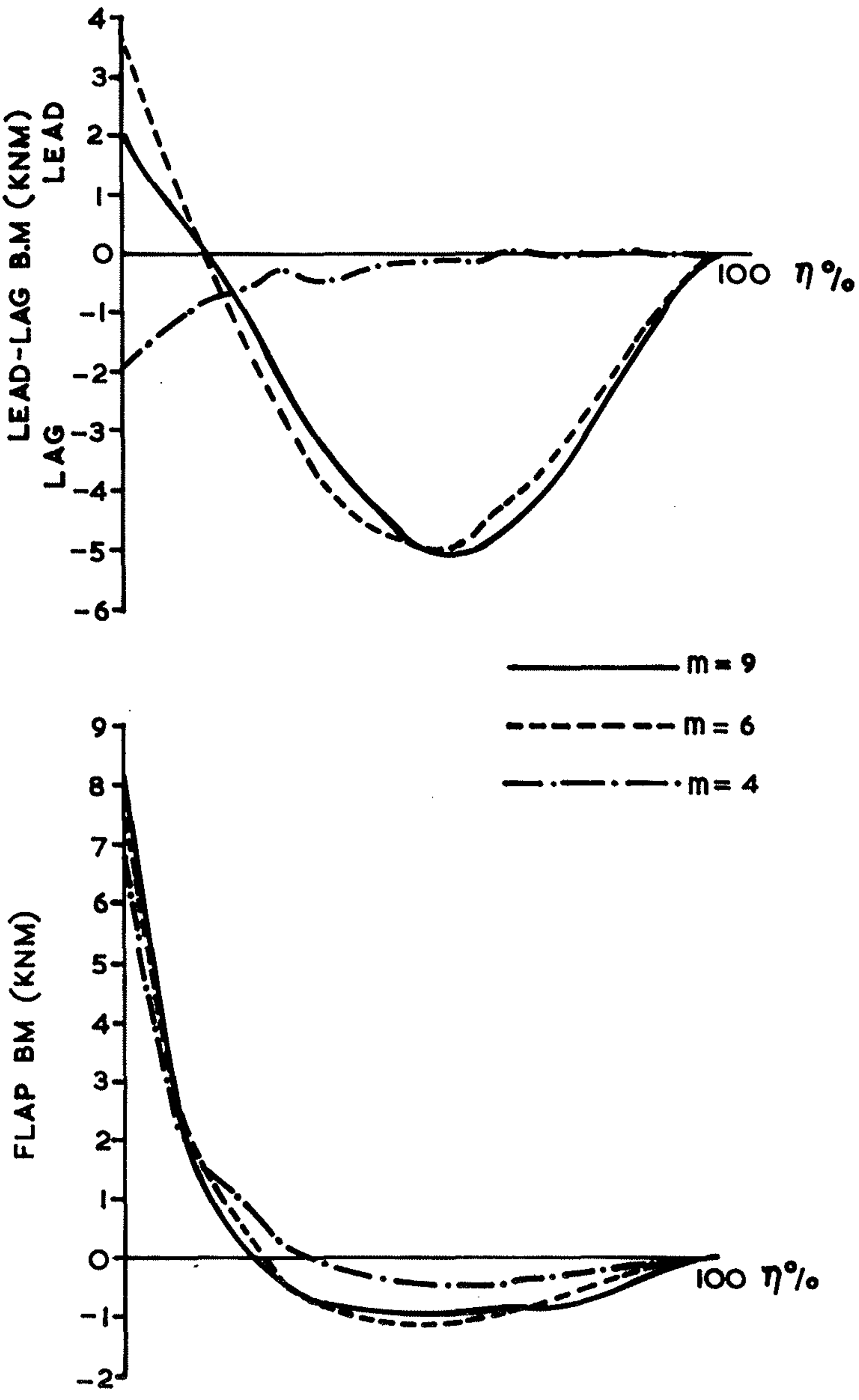

FIG. 3 LEAD-LAG AND FLAP BENDING MOMENTS IN THE HOVER STATE WITH NUMBER OF RETAINED MODES AS THE PARAMETER (DISC LOADING = 40KN, NB=4, Ω=34·17 RAD/S)